SCEC Award Number 25103
Integrated geodetic study of creep events on the Imperial Fault
Final Report

PI, Kathryn Materna[1]
Compiled by M. Morow Tan[1]; additional contributors Roger Bilham[1], Dan Gittins[1]
[1] *University of Colorado Boulder, Geological Sciences and CIRES*

Project Objectives

This study focuses on the Imperial Fault, one the of fastest partially-creeping faults in Southern California, accommodating the Pacific-North America plate boundary near the US-Mexico border. Previous studies have identified secular creep and creep events on the Imperial Fault (IF) in specific places using GNSS and creepmeter data (e.g., Goulty et al., 1978; Lyons et al., 2002; Lindsey and Fialko, 2016; Materna et al., 2024). These studies demonstrate that all four modes of creep are present on the IF: afterslip, triggered slip, continuous creep, and episodic creep. However, the typical point-based measurements of the prior work have spatial limitations, reducing our ability to determine the upper bound of slip and the extent of creep on faults (i.e., creepmeters typically represent a fraction of the total slip due to broader zones of deformation outside of the creepmeter sampling area).

This study leverages 10 years of Sentinel-1 InSAR data, increasing our spatial and temporal resolution of creep on the Imperial Fault. Using InSAR images, we visually identify creep on the Imperial Fault [IF], a dip-slip splay we call the W. Mesquite Fault [WMF], as well as the nearby Brawley Fault [BF]. Through Bayesian analysis, we estimate slip and depth of these creep events to develop scaling relationships between the kinematic rupture parameters of creep events.

Methodology

Sentinel-1 InSAR data (descending track 173; Copernicus Sentinel data) from January 2015 – November 2024 were processed using ISCE 2 (Rosen et al., 2012), yielding 265 12-day pair images. We visually inspect images for creep events and take profiles across the creep signals. We measure the length of the creep signal at the surface and assume this is the length of the rectangular fault source.

These profiles are inputted into a Python code developed by graduate student MT which simulates elastic dislocations using the formulation of Okada due to a finite rectangular fault source (Okada, 1985; Okada, 1992). We assume that the IF is a vertical fault with purely right-lateral slip, and that the WMF is a normal fault with unknown dip and rake of -90°. We also assume that slip during each creep event extends from the surface to an unknown depth, termed the “width” of the slipping patch. Using Markov Chain Monte Carlo (MCMC) sampling from the

PyMC software (Abril-Pla et al., 2023), posterior probability distributions of parameters (i.e. slip, dip, width) are evaluated with their respective uncertainties for each creep event. The models also estimate a linear slope and offset for each InSAR profile, which represent the typical InSAR ramp removal and reference pixel selection for the 1-D profile. If creepmeter data or other geological information exist for a creep event, we incorporate those into our priors.

Results

We identified a total of 18 creep events in the integrated geodetic data from InSAR, GNSS, and creepmeter records between January 2015 and November 2024 (Figure 1). We found in every case that the three geodetic techniques were highly self-consistent: each creepmeter or GNSS event was observed visually in InSAR interferograms (example given in Figure 2). This demonstrates the ability to use C-band InSAR to monitor creep events even in the highly vegetated Imperial Valley, which was not possible before the launch of Sentinel-1 (i.e., Lindsey and Fialko, 2016).

We select four well-recorded creep events to model (Figure 3): January 5-17, 2018 [on the IF]; June 29 – July 11, 2019 [WMF]; December 17-29, 2023 [BF]; and February 3-15, 2024 [WMF]. Modeling of the 2018 creep event on the IF indicates 1.6 ± 0.3 cm of slip but is poorly sensitive to width of the slip patch. The slip amount agrees with nearby creepmeter data, which recorded ~1.7 cm of slip for this creep event (unpublished, R. Bilham).

The June 29 – July 11, 2019 InSAR image records triggered creep on all three faults from the July 4 (M6.4) and July 5 (M7.1) Ridgecrest sequence, an example of dynamic triggering that was previously unknown. The Ridgecrest sequence occurred ~400 km from the Imperial Fault; this observation represents possibly the longest range of triggered creep observed on the IF, despite a long history of known triggered creep (i.e., from the 1992 M7.3 Landers earthquake and 1999 M7.1 Hector Mine earthquake).

The model of the 2023 creep event on the Brawley Fault estimates a shallow ($20° \pm 4°$) westward dipping plane, which disagrees with previous literature that states a near vertical dip. Slip and dip have a large trade-off, while the model is insensitive to width. Dip angle inconsistency and insensitivity to width may be due to a more complicated geometry near the intersection of the east and west fault splays, where the InSAR profile was taken. We find three additional creep events, including triggered creep from Ridgecrest, of varying length and locations on the east and west strands of the Brawley Fault.

Our modeling results show that the depth of creep is shallower on the W. Mesquite Fault (0.7-1.2 km) than the IF and predominantly normal motion, in agreement with the extensional Mesquite Basin caused by the interaction between the IF and Brawley Fault. The depth of creep on the central IF from our model is estimated to be deeper, ~3 km. Previous work by Lindsey and Fialko, 2016 estimate the velocity-strengthening sedimentary layer begins at ~4.25 km, which they interpret as the depth extent of shallow creep. This coincides with sediment depths of 4-4.5 km estimated from seismic refraction (Fuis et al., 1984). All our MCMC models of creep events estimate average width of the slip patch to be in the upper 3.5 km of the crust. Additionally, we do not find a trend in changing depth of creep over time, which may have indicated if the fault was strengthening or weakening. Finally, locations of creep identified in InSAR overlap each other, suggesting that creep on the IF is not segmented.

Using the relationship between slip and area of the slipping plane (Segall, 2010), we can calculate strain drop, and we find these creep events release on average 9.8 microstrain. In comparison, the background strain in the Imperial Valley is ~600 nanostrain/year (Crowell et al, 2013). From this first-order calculation, each creep event releases ~16 years of accumulated strain.

Further Work

Two creepmeters will be installed on the east and west strands of the Brawley Fault in March 2026. Creepmeter data will provide constraints on slip (as well as the length of the rectangular patch projected to the surface); in conjunction with additional InSAR data, it can be inputted into the developed MCMC code.

Future work may involve kinematic modeling to understand the effect of different fault geometries and creep locations. Due to oblique extension producing thin, warm crust in this region, and high sedimentation rates around the Salton Sea, seismicity analysis and geomorphic studies are of interest to understand how this pull-apart basin and the southern San Andreas may evolve.

Professional Outcomes

Graduate student MT presented a poster at the SCEC annual meeting, titled "Kinematics of creep events on the Imperial Fault". Prior to the start of the annual meeting, PI KM and MT visited sections of the Imperial, Brawley, and W. Mesquite Faults in preparation for future work in this region. The project is currently being developed towards a paper and technical presentation during MT's Comprehensive Exam in academic year 2026-2027.

Figures

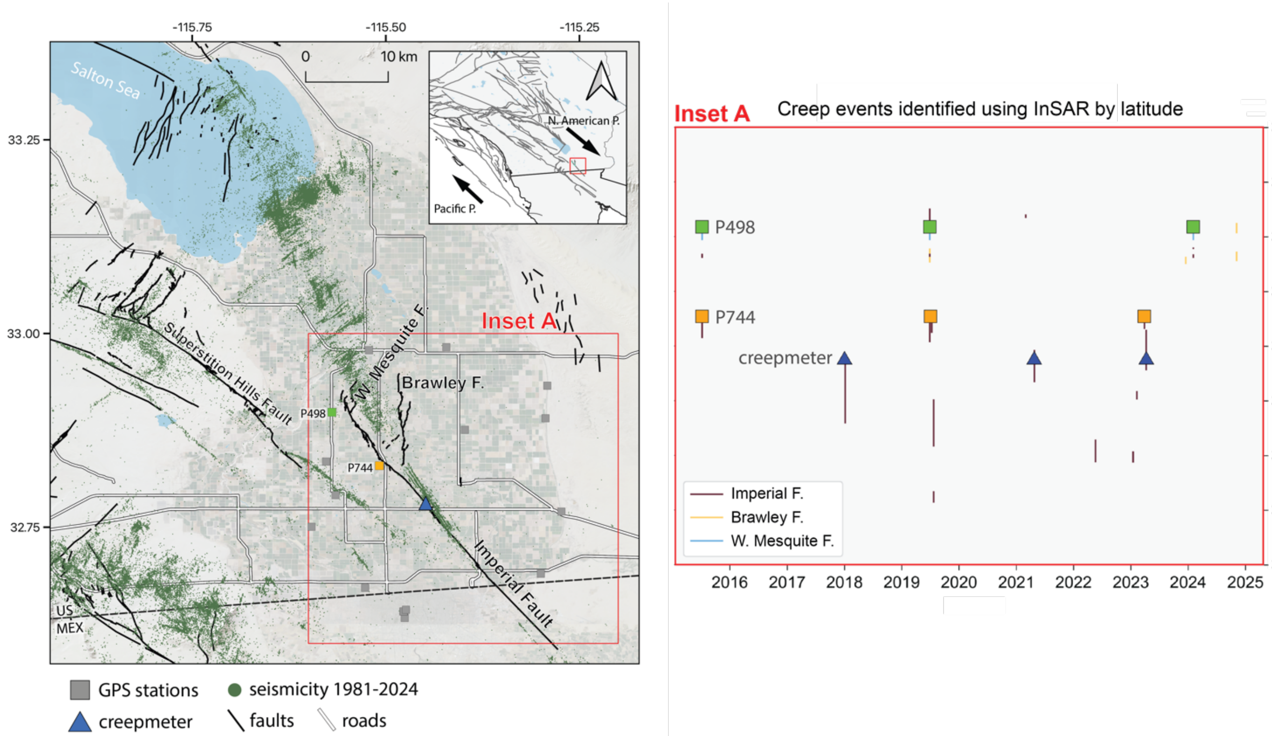

Figure 2: Map of study region, regional faults (QFFD; Salton Flats from Brothers et al., 2009), seismicity (SCEDC relocated catalog 1981-2014), and locations of GNSS stations and creepmeters. Inset A) catalogue of creep events identified using Sentinel-1 descending interferograms by latitude and fault. Symbols of GNSS and creepmeter indicate the instrument recorded creep.

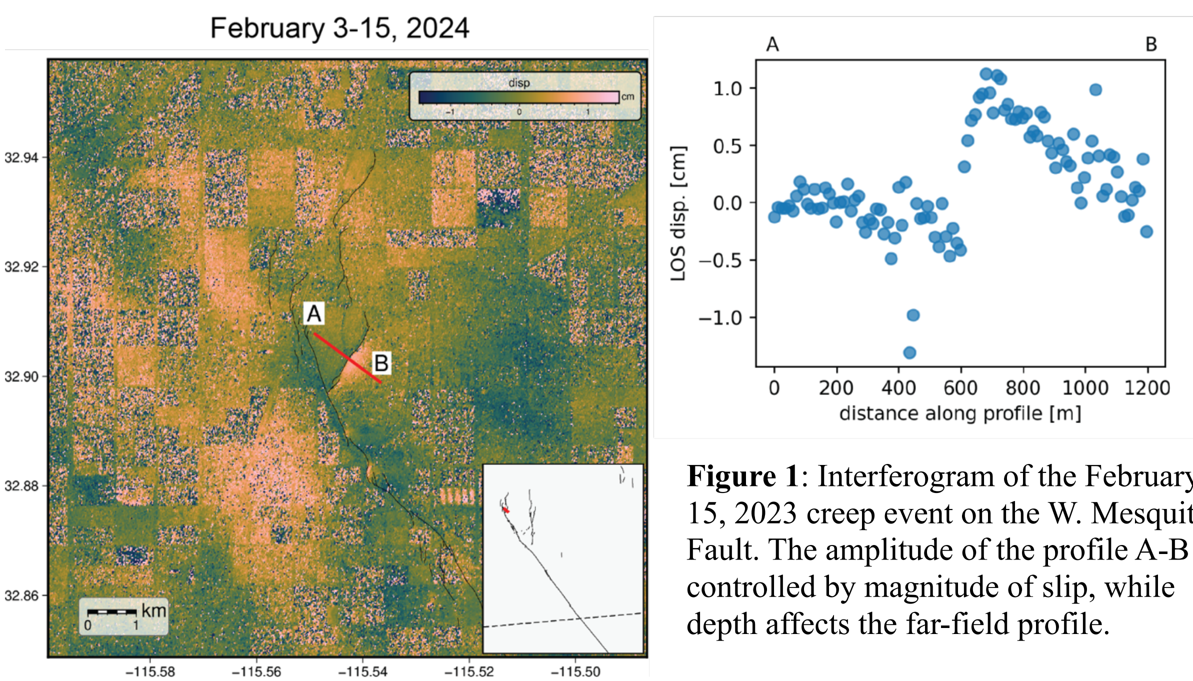

Figure 1: Interferogram of the February 3-15, 2023 creep event on the W. Mesquite Fault. The amplitude of the profile A-B is controlled by magnitude of slip, while depth affects the far-field profile.

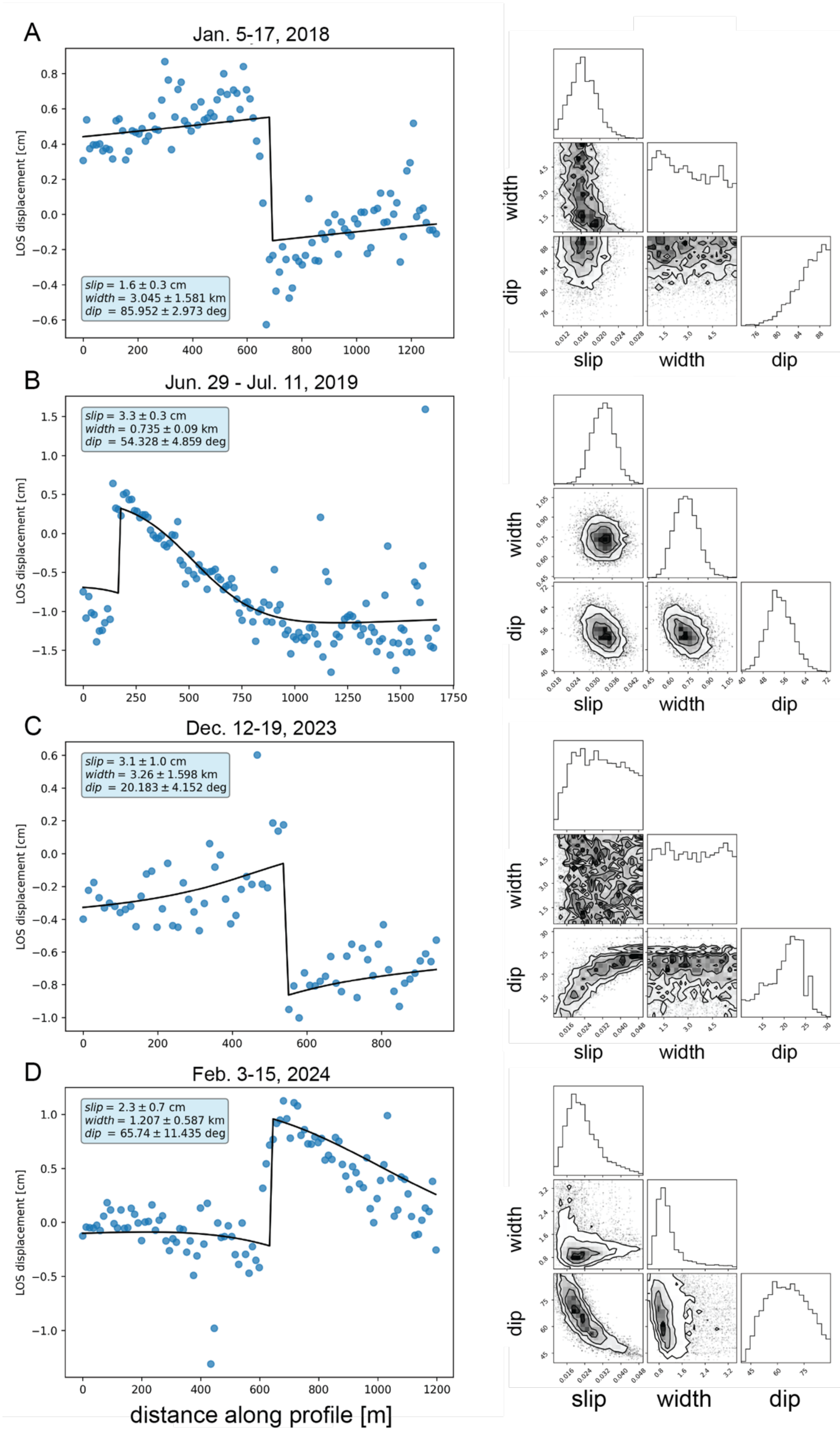
A
Jan. 5-17, 2018
slip = 1.6 ± 0.3 cm
width = 3.045 ± 1.581 km
dip = 85.952 ± 2.973 deg
LOS displacement [cm]
B
Jun. 29 - Jul. 11, 2019
slip = 3.3 ± 0.3 cm
width = 0.735 ± 0.09 km
dip = 54.328 ± 4.859 deg
LOS displacement [cm]
C
Dec. 12-19, 2023
slip = 3.1 ± 1.0 cm
width = 3.26 ± 1.598 km
dip = 20.183 ± 4.152 deg
LOS displacement [cm]
D
Feb. 3-15, 2024
slip = 2.3 ± 0.7 cm
width = 1.207 ± 0.587 km
dip = 65.74 ± 11.435 deg
LOS displacement [cm]
distance along profile [m]
width
dip
slip
width
dip

Figure 3: Results of best fitting parameters from MCMC sampling of elastic dislocations for four selected creep events. Blue circles represent profiles of creep taken from Line-of-sight InSAR data. The black line represents the Okada elastic dislocation model using the mean slip, dip, and width estimated from MCMC sampling. All priors are uniform distributions, unless otherwise noted. A) Priors were chosen based on creepmeter data and average dip (truncated normal distribution). Model is sensitive to slip and least sensitive to width. B) Model is sensitive to slip, width, and dip. C) Model has strong trade-offs between slip and dip, and is least sensitive to width. D) Model is sensitive to slip, width, and dip and has strong trade-offs between variables.

References

Abril-Pla, O., Andreani, V., Carroll, C., Dong, L., Fonnesbeck, C. J., Kochurov, M., Kumar, R., Lao, J., Luhmann, C. C., Martin, O. A., Osthege, M., Vieira, R., Wiecki, T., & Zinkov, R. (2023). PyMC: A modern, and comprehensive probabilistic programming framework in Python. *PeerJ Computer Science*, *9*, e1516. https://doi.org/10.7717/peerj-cs.1516

Brothers, D. S., Driscoll, N. W., Kent, G. M., Harding, A. J., Babcock, J. M., & Baskin, R. L. (2009). Tectonic evolution of the Salton Sea inferred from seismic reflection data. *Nature Geoscience*, *2*(8), 581–584. https://doi.org/10.1038/ngeo590

Crowell, B. W., Bock, Y., Sandwell, D. T., & Fialko, Y. (2013). Geodetic investigation into the deformation of the Salton Trough. *Journal of Geophysical Research: Solid Earth*, *118*(9), 5030–5039. https://doi.org/10.1002/jgrb.50347

Fuis, G. S., Mooney, W. D., Healy, J. H., McMechan, G. A., & Lutter, W. J. (1984). A seismic refraction survey of the Imperial Valley Region, California. *Journal of Geophysical Research: Solid Earth*, *89*(B2), 1165–1189. https://doi.org/10.1029/JB089iB02p01165

Goulty, N. R., Burford, R. O., Allen, C. R., Gilman, R., Johnson, C. E., & Keller, R. P. (1978). Large creep events on the Imperial fault, California. *Bulletin of the Seismological Society of America*, *68*(2), 517–521. https://doi.org/10.1785/BSSA0680020517

Lindsey, E. O., & Fialko, Y. (2016). Geodetic constraints on frictional properties and earthquake hazard in the Imperial Valley, Southern California. *Journal of Geophysical Research: Solid Earth*, *121*(2), 1097–1113. https://doi.org/10.1002/2015JB012516

Lyons, S. N., Bock, Y., & Sandwell, D. T. (2002). Creep along the Imperial Fault, southern California, from GPS measurements. *Journal of Geophysical Research: Solid Earth*, *107*(B10). https://doi.org/10.1029/2001JB000763

Materna, K., Bürgmann, R., Lindsay, D., Bilham, R., Herring, T., Crowell, B., & Szeliga, W. (2024). Shallow Slow Slip Events in the Imperial Valley With Along-Strike Propagation. *Geophysical Research Letters*, *51*(12), e2023GL108089. https://doi.org/10.1029/2023GL108089

Materna, K., & Wong, J. (2023). *Elastic_stresses_py* (Version 1.0.0) [Python]. https://doi.org/10.5281/zenodo.7951979

Meltzner, A. J., Rockwell, T. K., & Owen, L. A. (2006). Recent and Long-Term Behavior of the Brawley Fault Zone, Imperial Valley, California: An Escalation in Slip Rate? *Bulletin of the Seismological Society of America*, *96*(6), 2304–2328. https://doi.org/10.1785/0120050233

Okada, Y. (1985). Surface deformation due to shear and tensile faults in a half-space. *Bulletin of the Seismological Society of America*, *75*(4), 1135–1154. https://doi.org/10.1785/BSSA0750041135

Okada, Y. (1992). Internal deformation due to shear and tensile faults in a half-space. *Bulletin of the Seismological Society of America*, *82*(2), 1018–1040. https://doi.org/10.1785/BSSA0820021018

Rosen, P. A., Gurrola, E., Sacco, G. F., & Zebker, H. (2012). The InSAR scientific computing environment. *EUSAR 2012; 9th European Conference on Synthetic Aperture Radar*, 730–733.

Segall, P. (2010). *Earthquake and Volcano Deformation*. Princeton University Press.

Sharp, R. V., & Lienkaemper, J. J. (1982). Preearthquake and postearthquake near-field leveling across the Imperial Fault and the Brawley Fault zone. In C. E. Johnson, C. Rojahn, & R. V. Sharp (Eds.), *The Imperial Valley, California, Earthquake of October 15, 1979* (Vol. 1254, pp. 169–182). U.S. Gov.